Hard turbulence in rotating Rayleigh-Bénard convection

K. Julien,[1,2] S. Legg,[1,3] J. McWilliams,[2,3] and J. Werne[2]
[1]*Joint Institute for Laboratory Astrophysics, University of Colorado, Boulder, Colorado 80309*
[2]*National Center for Atmospheric Research, Boulder, Colorado 80307*
[3]*University of California, Los Angeles, Los Angeles, California 90095-1565*
(Received 10 April 1995)

We report a transition to hard turbulence in rapidly rotating Boussinesq convection at high Rayleigh and Taylor numbers. The probability density for vertical vorticity develops exponential tails, as in nonrotating hard-turbulent convection, whereas the temperature and velocity retain Gaussian distributions. The Nusselt-number scaling with Rayleigh number for the rotating hard-turbulent state is identical to that for nonrotating laboratory experiments, viz., $\mathrm{Nu}\sim\mathrm{Ra}^{2/7}$. [S1063-651X(96)50306-5]

PACS number(s): 47.27.Te, 47.32.Cc, 47.27.Cn, 47.27.Eq

Rayleigh-Bénard convection [1] is a common model problem for transitions to convective turbulence; the experiments of Libchaber and co-workers have delineated the transitions with increasing nondimensional Rayleigh number Ra [2–5]. The hard-turbulent state at high Ra has drawn much attention [6]; nevertheless, only recently (and partly through this work) has it been seen as an ubiquitous convective state, with manifestations spanning both large and small aspect ratio [2–5], two-dimensional (2D) flows [7], and even a side-heated geometry [8]. Here we report an example of hard turbulence in a strongly rotating fluid of geophysical and astrophysical relevance with detailed dynamics dramatically different from the nonrotating case. This discovery sheds light on the workings of hard turbulence and aids in evaluating theories for convective heat transport.

We integrate the Navier-Stokes equations for a rotating Boussinesq fluid [1] using a pseudospectral Fourier (horizontally periodic) Chebyshev (vertically bounded) tau method [9]. The top and bottom surfaces have fixed temperature with either no-slip or stress-free velocity conditions. Time integration is by a third-order, hybrid-implicit on-explicit Runge-Kutta scheme [10] in which the nonlinear and Coriolis terms are treated explicitly and the remaining linear terms implicitly. Pressure boundary conditions are satisfied simultaneously with the velocity, using the influence matrix method [11], and the resulting Chebyshev-truncation errors are removed with the tau correction [11]. The solutions have $\sigma=1$ (σ is the Prandtl number), an aspect ratio of 2 (unless otherwise noted), and vertical gravity and rotation vectors; Table I lists the solution parameters. The resolution is chosen to resolve the Kolmogorov length scale. In addition, the thermal boundary layers are resolved with at least 12 collocation (grid) points. The linearly most unstable horizontal wave number k_0 increases with the Taylor number [1], $\mathrm{Ta}=(2\Omega L^2/\nu)^2$ (where Ω is the rotation rate, L is the depth of the fluid layer, and ν is the kinematic viscosity). For the highest Ta case ($\mathrm{Ta}=3.2\times10^8$), k_0 is many times larger than $3.117/L$, the value for nonrotating convection, and we switch to $A=1$ for computational efficiency; we have checked at the lower $\mathrm{Ta}=1.0\times10^8$ that solutions with $A=1$ and 2 have the same statistical behavior.

The transition to hard turbulence coincides with the spontaneous ejection of plumes from the diffusive thermal layers at the heated and cooled boundaries [2]. The dynamics of these plumes has been invoked both directly [3] and indirectly (through the boundary-layer shear in the large-scale circulation they organize) [12] to explain the heat-transport law $\mathrm{Nu}\sim\mathrm{Ra}^{2/7}$. To examine how strong external rotation modifies these dynamics, we choose cases with comparable rotation and buoyancy time scales for all Ra. Thus, we fix the ratio $t_R/t_B=Ro=0.75$, where $t_R=(2\Omega)^{-1}$ is the rotation time, $t_B=\sqrt{L/(g\alpha\Delta)}$ is the buoyancy free-fall time (i.e., the time required for a parcel of temperature $\Delta/2$ to travel a distance L under gravitational acceleration g; α is the thermal expansion coefficient), and $\mathrm{Ro}=\sqrt{\mathrm{Ra}/(\sigma\mathrm{Ta})}$ is the convective Rossby number. Here Δ is the temperature difference imposed across the layer. For $\mathrm{Ra}\gtrsim10^6$, our solutions possess the scaling exponents $\gamma=0.431\pm0.005$ (0.435 ± 0.004) and $\beta=0.140\pm0.008$ (0.107 ± 0.004) for rms vertical velocity and temperature at midlayer for no-slip (stress-free) boundaries. For free-fall to be satisfied, $2\gamma=1-\beta$ [3]. The stress-free exponents satisfy this relation within two standard deviations, while the no-slip solutions obey it within one.

Our results may be summarized as follows. The flow is linearly unstable to steady rolls at $\mathrm{Ra}=4050$ (5074) for no-slip (stress-free) vertical boundaries, as predicted [1]. [For these low-Ra cases, we choose A equal to five times the wavelength of the most unstable linear mode at convective onset; $k_0=0.72/L$ ($0.89/L$) is the wave number.] Time dependence occurs immediately at onset in the form of the Küppers-Lortz transition with rolls losing their stability to oblique rolls oriented at finite angles, also as predicted [13]. As Ra is increased, coherent plumes begin to emerge from the thermal boundary layers: by $\mathrm{Ra}\approx6\times10^5$ strong peaks in the temperature skewness $\langle(T-\langle T\rangle)^3\rangle/T_{\mathrm{rms}}^3$ at the edge of the boundary layers indicate the plumes ($\langle\ \rangle$ denotes horizontal- and time-averaging). A striking feature of the plumes in this rotating environment is their strong cyclonic relative vorticity [14], which develops as they horizontally shrink due to boundary-layer convergence and thus spin-up to conserve absolute angular momentum. Their ensuing dynamics in the interior is dominated by vortex-vortex interactions [15] with neighboring plumes, which is so efficient in lateral mixing that a substantial negative temperature gradient $-\partial_z T\sim0.2\Delta/L$ ($0.25\Delta/L$) is sustained [16,17]. In addi-

TABLE I. Simulation parameters. $\mathrm{Ra_{crit}}$ and k_0 (L^{-1}) are the critical Ra and wave vector associated with Ta. ''Spectral modes'' refer to $x\times y\times z$, with z vertical. t $[L^2/(4\kappa)]$ and W_{rms} $(2\kappa/L)$ are the integration time after transients have subsided and the rms vertical velocity at midlayer. The maximum Courant-Friedrichs-Levy number, $\mathrm{CFL}=\delta t U/\delta r$, is 0.7 for the three-level Runge-Kutta time step δt; δr and U are the grid spacing and velocity. The number of ''turnover'' times simulated for a single ''convection cell'' is $tW_{\mathrm{rms}}/4(1+\pi/k_0)$.

Ra	Ta	$\mathrm{Ra_{crit}}$	k_0	Spectral modes	Boundaries	t	W_{rms}
3.09×10^4	5.50×10^4	1.17×10^4	6.5	$64\times64\times33$	no-slip	2.74	10.0
7.03×10^4	1.25×10^5	1.91×10^4	7.5	$96\times96\times49$	no-slip	1.58	15.2
2.81×10^5	5.00×10^5	4.55×10^4	9.6	$96\times96\times49$	no-slip	0.776	31.1
5.91×10^5	1.05×10^6	7.34×10^4	10.9	$96\times96\times49$	no-slip	0.455	44.6
2.53×10^6	4.50×10^6	1.91×10^5	14.2	$128\times128\times65$	no-slip	0.122	85.1
8.44×10^6	1.50×10^7	4.53×10^5	17.6	$128\times128\times65$	no-slip	0.0619	147.2
2.81×10^7	5.00×10^7	9.56×10^5	21.8	$192\times192\times97$	no-slip	0.0181	243.0
1.13×10^8	2.00×10^8	2.44×10^6	27.9	$384\times384\times193$	no-slip	0.00551	438.8
5.63×10^4	1.00×10^5	2.13×10^4	8.6	$96\times96\times49$	stress-free	2.99	14.8
1.97×10^5	3.50×10^5	4.70×10^4	10.7	$96\times96\times49$	stress-free	1.74	29.9
5.63×10^5	1.00×10^6	9.22×10^4	12.9	$128\times128\times65$	stress-free	0.479	51.0
1.97×10^6	3.50×10^6	2.08×10^5	15.9	$192\times192\times97$	stress-free	0.197	93.2
5.63×10^6	1.00×10^7	4.15×10^5	19.0	$192\times192\times97$	stress-free	0.0854	145.9
1.97×10^7	3.50×10^7	9.47×10^5	23.5	$256\times256\times129$	stress-free	0.170	252.0
5.63×10^7	1.00×10^8	1.90×10^6	28.0	$256\times256\times129$	stress-free	0.0155	402.4
1.78×10^8	3.16×10^8	4.07×10^6	34.0	$256\times256\times257$	stress-free	0.00749	660.0

tion, with no-slip boundaries the ejection of the strongly vortical plumes from the boundary layers is enhanced by Ekman pumping [18], most striking in the vertical-velocity skewness which is negative within nonrotating boundary layers [19], but is positive here. Despite these fundamental differences from the dynamics in nonrotating convection, the rotating solutions nevertheless exhibit hard-turbulent behavior at large Ra.

Figure 1 is $\mathrm{Nu}-1$ versus Ra for both no-slip and stress-free cases. The no-slip results are consistent with the 2/7 law for $\mathrm{Ra}>10^6$. The stress-free solutions, on the other hand, are consistent with $\mathrm{Ra}^{1/3}$ (i.e., the ''classical'' law proposed by Priestley [20]) in the range $10^6<\mathrm{Ra}<4\times10^7$, then undergo a transition to a less efficient heat-transport rate at higher Ra. Given that Ta is different for each Ra, we conclude that $\mathrm{Nu}\sim\mathrm{Ra}^{2/7}\mathcal{F}(\mathrm{Ro})$ at low Ro for the no-slip solutions, where $\mathcal{F}$ is an as yet undetermined function. We might expect $\mathcal{F}$ to be a decreasing function since rotation will enhance Nu slightly through the Ekman pumping associated with vortical plumes as proposed from laboratory experiments [21]. Our present evidence indicates that $\mathcal{F}$ is at most a weak function, but we are not yet prepared to declare its form.

In contrast to the Nu-Ra scaling, for which only the no-slip solutions exhibit hard-turbulent behavior, both no-slip and stress-free solutions undergo a transition to exponential probability density functions (PDFs) often associated with hard turbulence, albeit only for vorticity, not temperature as with nonrotating convection. Figure 2 shows midplane PDFs of vertical vorticity for $\mathrm{Ra}=5.9\times10^5$, 2.5×10^6, and 1.1×10^8 (5.6×10^5, 2.0×10^6, and 1.8×10^8) for no-slip (stress-free). The lowest Ra solutions exhibit skewed distributions with an exponential cyclonic tail and a weaker anticyclonic tail closer to Gaussian. The cyclonic skewness and strong intermittency result from angular momentum conservation of the plumes ejected at horizontally convergent sites in the boundary layers. As Ra increases, the anticyclonic tail also develops an exponential shape as turbulent midplane motions redistribute cyclonic vorticity. This transition is reminiscent of that for temperature PDFs in nonrotating convection.

Despite this transition in the vorticity field at high Ra, the midplane PDFs for T and $\vec{v}$ remain Gaussian, in contrast to the nonrotating case [2,7], at least up to the $\mathrm{Ra}\leqslant1.8\times10^8$ we have explored. If we take the view that exponential PDFs are merely indicative of a highly structured field, the thermal field remains Gaussian while the vorticity field does not because the vortical interactions between plumes rapidly rob them of their thermal content through mixing and dilution [17], leading to a weakly structured T field. The dilution of

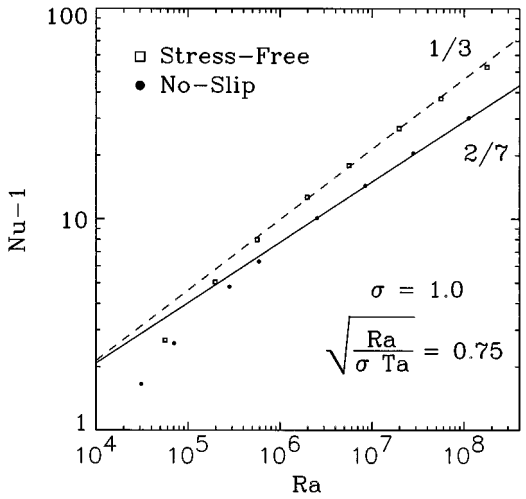

FIG. 1. Convective heat flux $\mathrm{Nu}-1$ versus Ra. The uncertainty in the data points is roughly the size of the symbols and results from the finite length of the runs. The solid (dashed) line corresponds to a 2/7 (1/3) power law with arbitrary normalization.

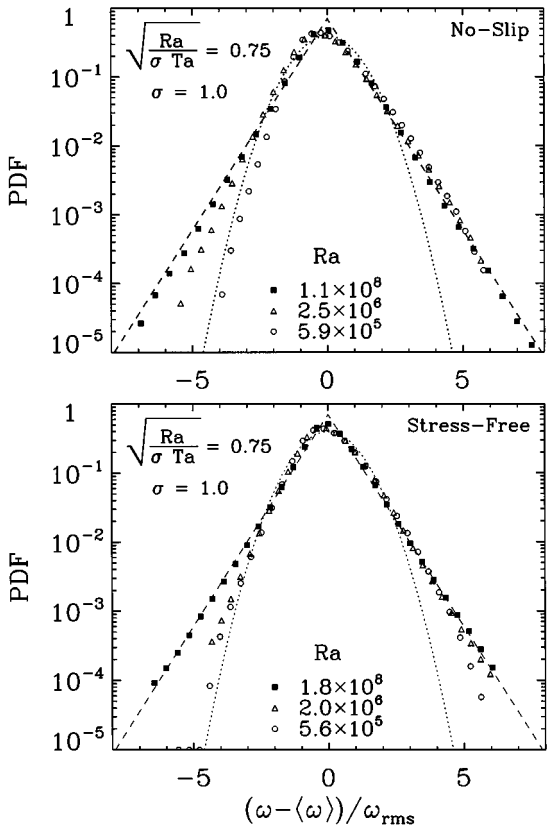

FIG. 2. Probability density functions (PDFs) for vertical vorticity ω. For Ra between 6×10^5 and 10^8, the PDF exhibits a continuous transition from Gaussian to exponential form for the anticyclonic tail (exponential cyclonic tails exist for all $\mathrm{Ra}>6\times10^5$). Gaussian (dotted) and exponential (dashed) distributions with zero mean and unit variance are shown.

the vorticity field is weaker because it is more strongly concentrated in the vortex core region than is T, and the mixing process primarily affects regions outside the cores. In fact, when vortex-merger events take place, the net effect is to *enhance* the circulation, not dilute it [15]. Vortex-stretching during plume ejection acts to concentrate the vorticity in the core region of a plume, leaving a portion of the plume's thermal content in the vortex periphery where it is susceptible to mixing. This view of different mixing dynamics for T and vorticity can be tested for $\sigma\gg1$, where the length scale for viscous effects exceeds that for diffusion. Laboratory experiments on rotating convection with silicone oil ($\sigma\approx8.4$) indicate that T PDFs remain Gaussian at least up to $\mathrm{Ra}\leqslant3.7\times10^{11}$ when $\mathrm{Ro}=0.75$ [22]. Having Gaussian PDFs for $\vec{v}$ and exponential PDFs for vorticity is similar to behavior in turbulent shear flows [23]; hence, velocity derivatives are seen to be more intermittent than the velocity itself.

The fact that rotating convection exhibits $\mathrm{Nu}\sim\mathrm{Ra}^{2/7}$ for no-slip boundaries, but gives $\mathrm{Nu}\sim\mathrm{Ra}^{1/3}$ for a limited range in Ra for stress-free, sheds light on the means by which heat is transported in hard turbulence. All of the general features assumed in the qualitative scaling theory of Castaing *et al.* [3] are present here: thermal boundary layers (through which all of the heat flux is diffusive), a turbulent interior (described by free-fall arguments), and an intermediate ''mixing zone'' (within which plumes are first formed, then destroyed by turbulent motions as they travel vertically due to buoyancy). In fact, because of the efficient lateral mixing in our rotating solutions, the term ''mixing zone'' is even more appropriate for our solutions than the nonrotating case. Thus, one might imagine that [3] is sufficiently general to encompass nonrotating *and* rotating convection. On the other hand [3], would also predict $\mathrm{Nu}\sim\mathrm{Ra}^{2/7}$ for stress-free solutions, as well as no-slip. Because our stress-free results initially exhibit $\mathrm{Nu}\sim\mathrm{Ra}^{1/3}$, we conclude that the nature of the velocity conditions is important for the 2/7 law. In fact, this result supports the alternate theory proposed by Shraiman and Siggia [12] which derives the 2/7 law based on the structure of the thermal and viscous boundary layers attached to a no-slip surface. Furthermore, of the four theories of hard turbulence currently in the literature [3,12,24], [12] is the only one supported by our results since it also is the only theory which distinguishes between no-slip and stress-free boundaries. However, the reduction in the heat-transport scaling between stress-free boundaries at high Ra is intriguing. What is the heat-transport law for rapidly rotating turbulent convection between stress-free boundaries for $\mathrm{Ra}>4\times10^7$? We cannot answer this yet because our highest Ra is not sufficient to allow a substantial range of exploration above $\mathrm{Ra}\approx4\times10^7$. It is interesting to note, however, that the Nu transition at $\mathrm{Ra}\approx4\times10^7$ occurs when the mean thermal boundary layer thickness λ equals the Ekman-layer thickness $\delta_E=[\nu/(2\Omega)]^{1/2}$ and therefore is likely controlled by rotational affects. (Convection over stress-free boundaries can possess Ekman layers if λ is not horizontally uniform [17,25].) In addition, making use of our observed scaling of δ_E and λ, we expect a similar crossover for the no-slip $\mathrm{Ro}=0.75$ solutions at $\mathrm{Ra}\approx10^{16}$.

It may seem a surprise that strongly rotating and nonrotating convection should transport heat in the same manner. This is especially striking considering the strong vortical interactions of plumes and the additional transport by Ekman pumping that exist in rotating convection, but not in nonrotating convection. One may expect significant departures as $\mathrm{Ro}\to0$: as Ta is increased, so is k_0 (see Table I) [26], leading to the possible loss of dominance of boundary-layer shear (between plumes) to the dynamics of plumes themselves. However, for $\mathrm{Ro}\lesssim1$, we have another convective regime whose instabilities, coherent structure dynamics, and boundary layers are all unique, which exhibits the exponential PDFs and 2/7 scaling seen in other fully developed regimes, indicating that the explanation for these phenomena does not lie in the specifics of the dynamics, but are generic features of fluid turbulence. Two features that *are* common to *all* physical regimes for which the 2/7 law is known to hold are (1) coherent plume structures capable of generating strong local shears and (2) no-slip boundaries (barring a further stress-free transition at larger Ra).

K.J. and S.L. are supported by the High Performance Computation and Communication Grant No. ECS9217394. Computations were carried out at the Pittsburgh Supercomputing Center (PSC) under Grant No. MCA935010P. NCAR is funded by the National Science Foundation.

[1] S. Chandrasekhar, *Hydrodynamic and Hydromagnetic Stability* (Clarendon Press, Oxford, 1961).

[2] F. Heslot, B. Castaing, and A. Libchaber, Phys. Rev. A **36**, 5870 (1987).

[3] B. Castaing, G. Gunaratne, F. Heslot, L. P. Kadanoff, A. Libchaber, S. Thomae, X.-Z. Wu, S. Zaleski, and G. Zanetti, J. Fluid Mech. **204**, 1 (1989).

[4] M. Sano, X.-Z. Wu, and A. Libchaber, Phys. Rev. A **40**, 6421 (1989).

[5] X.-Z. Wu and A. Libchaber, Phys. Rev. A **45**, 842 (1992).

[6] E. D. Siggia, Annu. Rev. Fluid Mech. **26**, 137 (1994), and references therein.

[7] E. E. DeLuca, J. Werne, R. Rosner, and F. Cattaneo, Phys. Rev. Lett. **64**, 2370 (1990); J. Werne, E. E. DeLuca, R. Rosner, and F. Cattaneo, *ibid.* **67**, 3519 (1991); J. Werne, Phys. Rev. E **48**, 1020 (1993); J. Werne (unpublished).

[8] A. Belmonte, A. Tilgner, and A. Libchaber, Phys. Rev. E **51**, 5681 (1995).

[9] C. Canuto, M. Y. Hussaini, A. Quarteroni, and T. A. Zang, *Spectral Methods in Fluid Dynamics* (Springer-Verlag, New York, 1988).

[10] P. R. Spalart, R. D. Moser, and M. M. Rogers, J. Comput. Phys. **96**, 297 (1991).

[11] L. Kleiser and U. Schumann, in *Proceedings of the Third Gesellschaft fur Angewandte Mathematik und Mechanik Conference Numerical Methods in Fluid Mechanics*, edited by E. H. Hirschel (Vieweg, Braunschweig, 1980), p. 165; J. Werne, J. Comput. Phys. **120**, 260 (1995).

[12] B. I. Shraiman and E. D. Siggia, Phys. Rev. A **42**, 3650 (1990).

[13] F. H. Busse and R. M. Clever, *Recent Developments in Theoretical and Experimental Fluid Mechanics* (Springer, New York, 1979); T. Clune and E. Knobloch, Phys. Rev. E **47**, 2236 (1993).

[14] Y. Nakagawa and P. Frenzen, Tellus **7**, 1 (1955); for another classic text, see Rossby, J. Fluid Mech. **36**, 309 (1969).

[15] H. Aref, Ann. Rev. Fluid Mech. **15**, 345 (1983); M. V. Melander, N. J. Zabusky, and J. C. McWilliams, J. Fluid Mech. **195**, 303 (1988); D. G. Dritschel and D. W. Waugh, Phys. Fluids **4**, 1737 (1992); J. C. McWilliams, J. Fluid Mech. **146**, 21 (1984).

[16] B. M. Boubnov and G. S. Golitsyn, J. Fluid Mech. **219**, 215 (1990).

[17] K. Julien, S. Legg, J. McWilliams, and J. Werne, J. Fluid Mech. (to be published).

[18] Ekman pumping occurs when a vortex tube terminates at a solid boundary. For a tube in geostrophic balance (i.e., with the radial pressure gradient balancing centrifugal acceleration), pumping of fluid away from the boundary occurs at the vortex core due to vanishing at the wall of the fluid velocity (and hence the centrifugal acceleration), creating a pressure imbalance. See, for example, A. E. Gill, *Atmosphere-Ocean Dynamics* (Academic Press, New York, 1975).

[19] C. H. Moeng and R. Rotunno, J. Atmos. Sci. **47**, 1149 (1990).

[20] C. H. B. Priestley, Austral. J. Phys. **7**, 176 (1954).

[21] F. Zhong, R. Ecke, and V. Steinberg, J. Fluid Mech. **249**, 135 (1993).

[22] J. E. Hart and D. R. Ohlsen (unpublished).

[23] B. Castaing, Y. Gagne, and E. J. Hopfinger, Physica D **46**, 177 (1990).

[24] Z.-S. She, Phys. Fluids A **1**, 911 (1989); V. Yakhot, Phys. Rev. Lett. **67**, 769 (1992).

[25] R. Hide, Tellus **16**, 523 (1964).

[26] The mean spacing between plumes is consistent with the most unstable horizontal scale predicted by linear stability. No domain-filling motion is observed.